CrossMark

Adsorption and regeneration characteristics of phosphorus from sludge dewatering filtrate by magnetic anion exchange resin

Mingyang Song[1] · Min Li[1]

Abstract

Removal and recovery of phosphorus (P) from sewage are essential for sustainable development of P resource. Based on the water quality determination of sludge dewatering filtrate from a wastewater treatment plant in Beijing, this study investigated the adsorption and regeneration characteristics of P by magnetic anion exchange resin (MAEX). The experiments showed that the P adsorption capacity of MAEX could reach a maximum of 2.74 mg/mL when initial P concentration was 25 mg/L and dosage of MAEX was 8 mL/L. The P adsorption on MAEX resin was suitable for large temperature range (283–323 K). However, the adsorption capacity was reduced in various degrees due to the interference of different anions (Br^-, SO_4^{2-}, Cl^-, NO_3^-, HCO_3^-, CO_3^{2-}) and organic compounds (bovine serum albumin, humic acid). Kinetics studies indicated that the P adsorption process followed the pseudo-second-order model. The MAEX resin had a rapid P adsorption rate and the P adsorption capacity at 30 min could reach 97.7–99.3% of q_e. Increase of temperature was favorable to P adsorption on MAEX, and the adsorption isotherm data fitted to Langmuir model more than Freundlich model. Meanwhile, the thermodynamics parameters were calculated; it was shown that the adsorption process was an endothermic reaction. Desorption and regeneration experiments showed that $NaHCO_3$ was a suitable regenerant, and the P adsorption capacity could reach 90.51% of the original capacity after 10 times of adsorption-desorption cycles; this indicated that MAEX resin has an excellent regeneration performance and thus has a very good application prospect of P removal and recovery. Fourier transform infrared spectroscopy (FTIR) analysis confirmed that ion exchange, charge attraction, and hydrogen bonding affected the removal of P by the MAEX resin. The vibrating sample magnetometer (VSM) analysis revealed that MAEX resin was a kind of soft magnetic materials with good magnetism.

Keywords Phosphorus · Magnetic anion exchange resin · Adsorption · Kinetics · Isotherm · Regeneration

Introduction

Phosphorus (P) is essential but non-renewable (Roy 2017). In nature, P only linearly moves from the land to the sea (Hao et al. 2010). Across the globe, P ore depletion is getting worse by relying on limited natural resources (Lwin et al. 2017). However, the unreasonable discharge of P with the domestic sewage and industrial wastewater leads to eutrophication, and it gradually becomes one of the research hotshots all over the world (Xu et al. 2014; Song et al. 2017). Therefore, not only for scanty P resources but also for serious P pollution, P recovery from sewage and sludge has become a particularly promising option (Schütte et al. 2015).

Massive sorts of P-recovery technologies have been researched and applied (Sartorius et al. 2012), including traditional chemical precipitation, crystallization, biological method, and adsorption, etc. (Morse et al. 1998; Shih et al. 2017; Yuan et al. 2012; Loganathan et al. 2014). Of these, the adsorption method is routinely described as a widely wastewater treatment option because of its easy operation, stable treatment effect, reversible process, low-cost absorbents (Bhatnagar and Sillanpää 2011; Dai et al. 2011). A variety of P adsorbents have been developed and evaluated, such as fly ash (Ugurlu and Salman 1998), slag (Ozacar 2003), MgMn-layered double hydroxides (Chitrakar et al. 2005), red mud (Huang et al. 2008), zirconium (Chitrakar et al. 2006), Fe-EDA-SAMMS (self-assembled monolayers on mesoporous supports, a registered trademark of Steward Advanced Materials) (Chouyyok et al. 2010), and palygorskite (Gan

et al. 2009). Recently, using magnetic anion exchange resin (MAEX) to remove pollution from water has attracted much attention.

MAEX is a strong base anionic resin with some ammonia functional groups and a magnetized component within its structure that enables this resin to act as a weak individual magnet (Mergen et al. 2008). In contrast with the traditional anion exchange resins, MAEX has two distinctive features. First, the particle size of MAEX, ranging from 150 to 180 μm, is small and the specific surface area is relatively large. This has contributed to rapidly adsorb the negative charge pollutants in water by MAEX (Boyer and Singer 2005). Second, the resin is applied to water and wastewater in a slurry form and will be mixed well with adsorbate by mechanical stirring, thus decreasing the resistance to liquid phase mass transfer (Liu et al. 2011). Initially, MAEX was designed specifically to remove the dissolved organic carbon (DOC) from wastewater, while it recently has become concerned to remove inorganic anions. MAEX had a sulfate removal ratio of 9–24% and a nitrate removal ratio of 17–42% (Kitis et al. 2007). Besides, MAEX had a good adsorption effect on P, while the removal rate was about 70% (Ding et al. 2012). However, the previous study was incomplete since neither the reutilization effect of resin nor the adsorption mechanism was evaluated and explored.

Accordingly, this study investigated the P adsorption and regeneration characteristics of MEAX based on the water quality determination of sludge dewatering filtrate from a wastewater treatment plant (WWTP) in Beijing. For this purpose, the effects of initial P concentration, adsorbent dosage, initial pH, temperature of solution, ion strength, coexistent anions, and organic compounds on P adsorption were investigated. Adsorption kinetics, isotherm, and thermodynamics were also performed. Moreover, the regeneration characteristics of MEAX were analyzed by exploring the kinds of regenerants and regeneration times. In addition, the characterizations of MAEX resin before and after adsorption were investigated by Fourier transform infrared spectroscopy (FTIR) and vibrating sample magnetometer (VSM). The outcomes will be important for providing the fundamental basis for practical application in P recovery by magnetic resin.

Materials and methods

Sampling and analysis of sludge dewatering filtrate

Sludge dewatering filtrate samples were obtained from a WWTP with the anaerobic-anoxic-oxic (A/A/O) process in Beijing. Then the samples were stored at 4 °C and transported to the laboratory.

Table 1 and Fig. 1 presented the water quality of the sludge dewatering filtrate samples. The amount of P in the filtrate was

Table 1 Water quality of sludge dewatering filtrate

Water-quality index	Average value	Standard deviation
Temperature (°C)	16	0.027
pH	7.25	0.001
ORP (mV)	94.95	0.000
DO (mg/L)	1.81	0.000
SS (mg/L)	1159	24.222
Total nitrogen (mg/L)	149.80	0.087
Ammonia nitrogen (mg/L)	1.10	0.000
tCOD (mg/L)	1414	88.667
sCOD (mg/L)	153	10.889
Total phosphorus (mg/L)	23.54	2.693
Soluble total phosphorus (mg/L)	19.76	0.297
Soluble orthophosphorus (mg/L)	19.42	0.964
Granular total phosphorus (mg/L)	3.78	1.211
Other soluble phosphorus (mg/L)	0.33	0.519

considerable and the proportion of soluble total P in total P was high. As shown in Fig. 1, tryptophanlike was the main organic pollutant, consistent with the research result of Liu et al. (2016). In the meantime, according to the amount of P in the water samples, the P concentration of the simulated wastewater in the follow-up experiments was determined to be 25 mg/L.

P adsorption experiments by MAEX resin

All MAEX resins, the adsorbent of this study, were purchased from Jiangsu Guochuang New Material Research Center with a wet superficial density of 1.058 g/mL. MAEX was stored in plastic bottle. Before using, it would be rinsed with deionized water for several times in order to remove impurities, then after settled for about 30 min, a certain amount of MAEX resin was used according to the adsorption experiment requirement.

Table 2 showed the size distribution of MAEX resin measured by Malvern Laser Particle Size Analyzer. The particle size of MAEX resin mainly ranged from 244 to 445 μm. The morphological features and the surface characteristics of MAEX resin were obtained by scanning electron microscopy (SEM), as shown in Fig. 2. From Fig. 2, we can conclude that the surface of MAEX resin appears to be ragged, due to Fe_2O_3 loaded on the surface of the resin for magnetic purpose.

Potassium dihydrogen phosphate (KH_2PO_4) was used as the adsorbate. KH_2PO_4 solutions and MAEX resin were added into a set of 50 mL conical flasks, and the flasks were sealed and agitated in an incubator for some time. Then the mixture was filtered by 0.45 μm membranes, and the P in filtrates was analyzed by the molybdenum blue colorimetry.
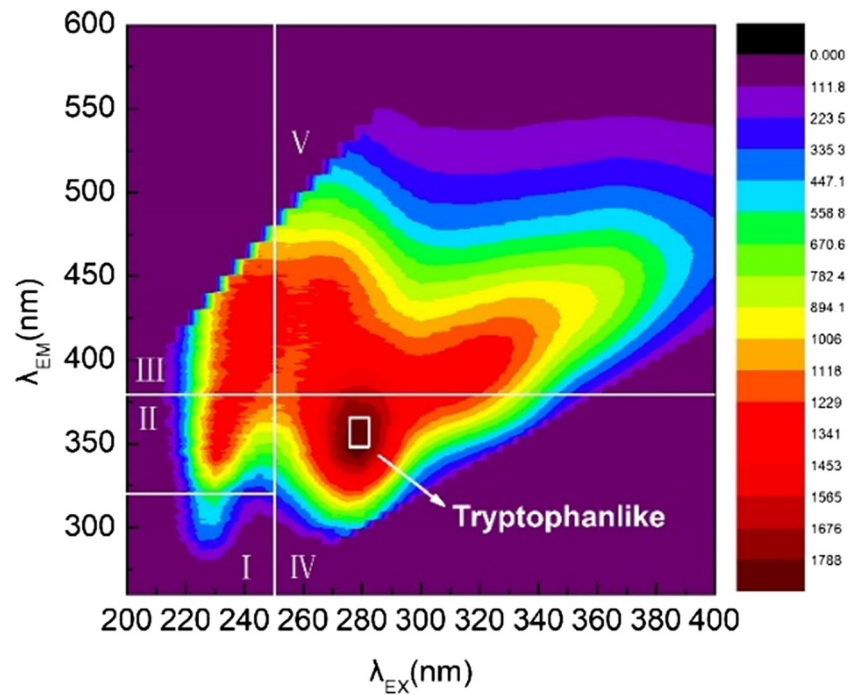
The P removal rate and the P adsorption capacity of MAEX resin were calculated as Eqs. (1) and (2), respectively:

$$E = \frac{C_0 - C_t}{C_0} \times 100\% \tag{1}$$

$$q_t = \frac{(C_0 - C_t)V}{W} \tag{2}$$

where C_0 and C_t stand for P concentration before and after adsorption (mg/L), W stands for dosage of MAEX resin (mL), and V stands for volume of the mixed solution (L).

The effect experiments of different factors on P adsorption by MAEX resin were employed by varying resin dosage, initial pH, temperature, ionic strength, co-existent anions, and organic compounds. The effect experiments of resin dosage were conducted with an electric mixer. However, as to accurately control the experimental parameters, the later experiments were conducted in a thermostatic oscillator. The initial pH values were adjusted by adding 0.1 mol/L NaOH or HCl if necessary.

Table 2 Size distribution of MAEX resin

No.	$D_x (10)/\mu m$	$D_x (50)/\mu m$	$D_x (90)/\mu m$
1	243.280	328.959	445.260
2	244.489	329.936	443.547
3	244.434	331.569	445.193
4	244.219	330.597	446.356
5	244.595	330.937	444.799
Average	244.197	330.400	445.031

Table 3 showed the experimental conditions from the effect experiments of different factors on P adsorption by MAEX resin.

Adsorption kinetic and thermodynamic experiments

Batch adsorption experiments were carried out to explore adsorption kinetics and diffusion mechanism. P solutions with different initial concentration (10 mg/L, 25 mg/L, and 50 mg/L) and 10 mL MAEX resin were added into a set of 500 mL beakers. The mixture was stirred using the motor agitators for 2 h when the adsorption reached equilibrium. In the meantime, the mixtures sampled from the beakers at regular intervals were filtered by 0.45 μm membranes, and the P concentration infiltrates were determined. Each experiment was performed three times under identical conditions.

As for the adsorption thermodynamic research, the experiments were conducted at pH 8, MAEX resin dosage of 8 mL/L, and shaking for 30 min, while the adsorption temperatures were 293, 303, and 313 K and the initial P concentrations were 5, 10, 15, 20, 25, 50, 100, 150, 200, and 250 mg/L. The amount of P adsorption at equilibrium, q_e (mg/mL), was computed as follows:

$$q_e = \frac{(C_0 - C_e)V}{W} \tag{3}$$

where C_0 and C_e are the initial and the equilibrium P concentrations (mg/L), respectively, V is the volume of the
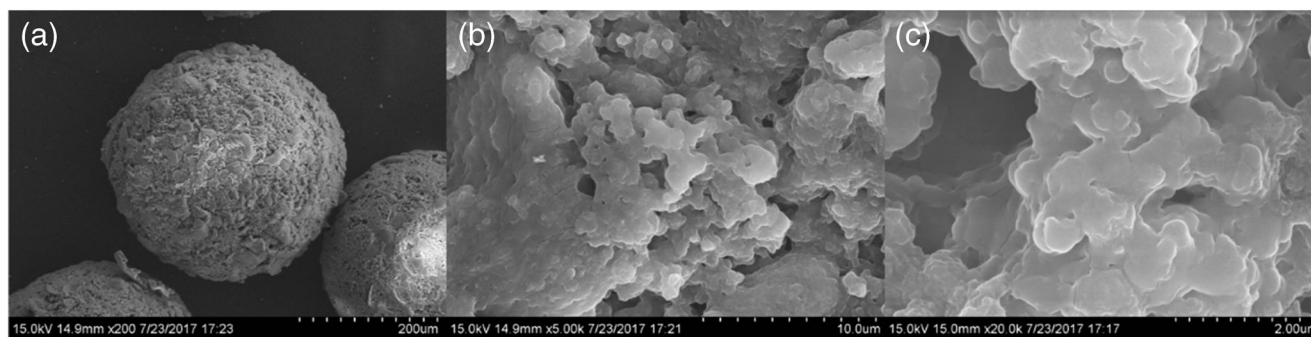
Fig. 2 SEM images of MAEX resin: **a** × 200; **b** × 5000; **c** × 20,000

solution (L), and W is the dosage of MAEX resin (mL). Thermodynamic parameters could be calculated by experiment data of the temperature effect on P adsorption by MAEX resin. Each experiment was also performed three times under identical conditions.

Regeneration study on MAEX resin

Regeneration experiments were first carried out with six different regenerants (H_2O, NaCl, Na_2CO_3, NaOH, HCl, and $NaHCO_3$) in the same concentration of 1.0 mol/L, and the adsorption capacities of MAEX resins after regeneration were compared to choose suitable regenerants. Then, the effect experiments of regenerant concentrations ($NaHCO_3$ and NaCl) were discussed. In order to investigate the stability and the readsorption capacity of MAEX resin, ten times of adsorption-desorption cycle experiments were carried out by using regenerants of $NaHCO_3$ and NaCl.

Regenerative effect of reagents for MAEX resin, E, was computed as follows:

$$E = \frac{q_R}{q_0} \tag{4}$$

where q_0 is the initial adsorption capacity of MAEX resin (mg/mL), and q_R is the adsorption capacity of MAEX resin after regenerated (mg/mL).

FTIR and VSM analysis

To further elucidate the process of P adsorption and the stability of MAEX resin, MAEX resin, before and after once adsorption, was characterized by Fourier transform infrared spectrometer (FTIR) and vibrating sample magnetometer (VSM). The FTIR spectrum was recorded at room temperature ranging from 400 to 4000 cm^{-1} by FTIR spectrometer (Vertex 70, Germany). The magnetic properties of MAEX

Table 3 The experimental parameters for different factor

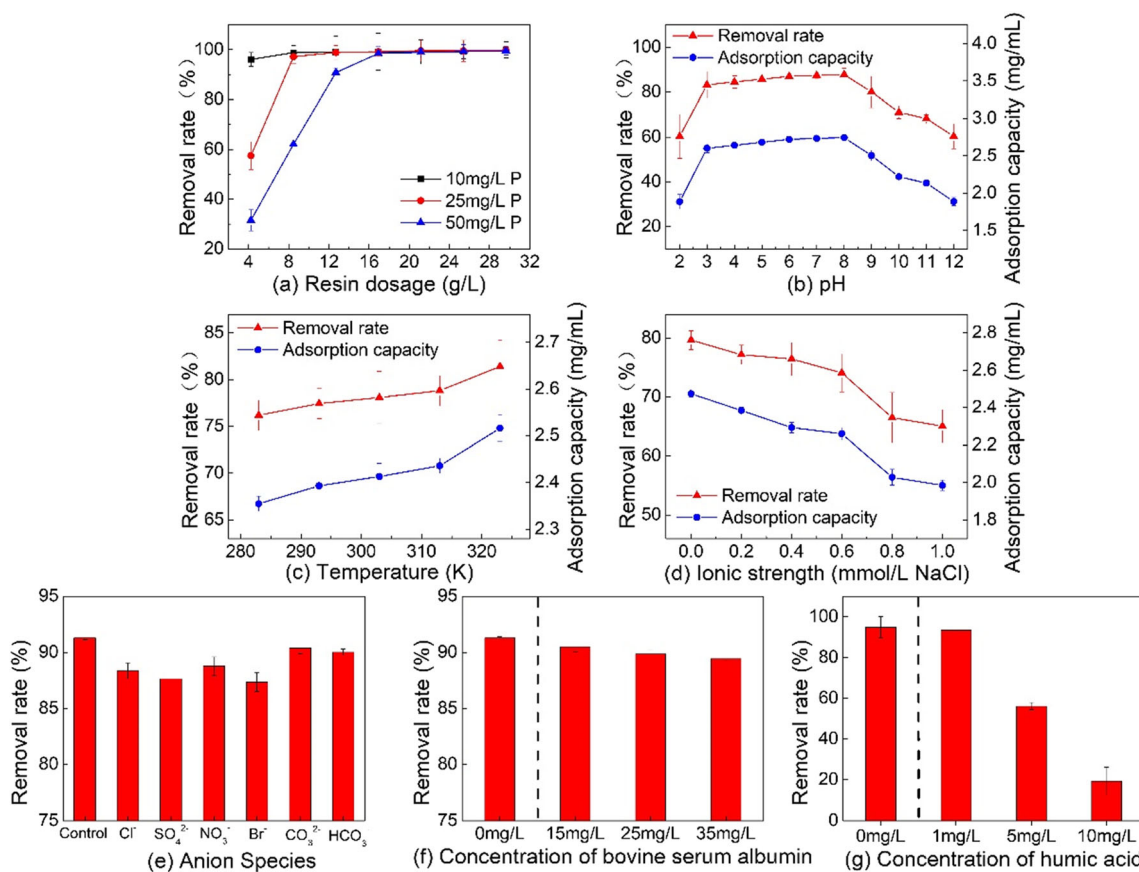| Experimental groups	Initial P concentration (mg/L)	Resin dosage (mL/L)	Initial pH	Temperature (K)	Ionic strength (mmol/L NaCl)	Coexistent anion	Concentration of bovine serum albumin (mg/L)	Concentration of humic acid (mg/L)
a	25	4, 8, 12, 16, 20, 24, 28	–	298	–	–	–	–
b	25	8	2, 3, 4, 5, 6, 7, 8, 9, 10, 11, 12	298	–	–	–	–
c	25	8	8	283, 293, 303, 313, 323	–	–	–	–
d	25	8	8	298	0.0, 0.2, 0.4, 0.6, 0.8, 1.0	Cl^-	–	–
e	25	8	8	298	–	Cl^-, SO_4^{2-}, NO_3^-, Br^-, CO_3^{2-}, HCO_3^-	–	–
f	25	8	8	298	–	–	0, 15, 25, 35	–
g	25	8	8	298	–	–	–	0, 1, 5, 10

Fig. 3 The influence of different factors on the adsorption of P by MAEX resin

resin were assessed with a multifunctional vibrating sample magnetometer (Versa Lab, USA).

Results and discussion

Effects of different parameters on P adsorption by MAEX resin

Monofactor experiments were carried out by the control variable method to investigate the effect of different factors on the P adsorption by MAEX resin.

From Fig. 3a, as the resin dosage was reached to 8 mL/L, it may be noted that there was no significant increase in the removal rate of P when the initial P concentration is 25 mg/L (closed to the P concentration in the actual sludge dewatering filtrate). The resin dosage of 8 mL/L was selected for the following experiments.

According to Fig. 3b, the suitable pH is 8 and the removal rate of P could reach to 87.8%. Besides, both the removal rate

and the adsorption capacity all increased first and then decreased as pH was increasing. The removal rate of P and the adsorption capacity of MAEX resin reached to the maximum at pH = 8. The existing state of phosphate in aqueous medium is closely related with pH of the solution. Under the condition of low pH value, phosphate mainly exists in the forms of H_3PO_4 and $H_2PO_4^-$ (Ozmen et al. 2011), and these two forms are more difficult to exchange the chloride ions from the active adsorption sites, which could lead to the low adsorption capacity of MAEX resin. In addition, since the pH of solution was mainly adjusted by hydrochloric acid or sodium hydroxide, the introduction of chloride ions into the solution can inhibit the exchange between phosphate and chloride. When the pH of solution increases to 8, phosphate mainly exists in the forms of HPO_4^{2-} and PO_4^{3-}. The increase of ionic charge can lead to the increase of ion exchange capacity between phosphate and chlorine at the active adsorption sites, resulting in the increase of the adsorption capacity. However, as the pH of solution increased to 12, the competitive adsorption between phosphate and hydroxyl ions in solution results in the

Table 4 The change of pH after adding anions		P	P + Cl⁻	P + SO₄²⁻	P + NO₃⁻	P + Br⁻	P + CO₃²⁻	P + HCO₃⁻
	pH	2.55	2.56	2.55	2.52	2.54	2.74	2.93

Table 5 Kinetic parameters of P adsorption on MAEX resin at different initial P concentrations

Pseudo-first-order

c_0 (mg/L)	$q_{e\text{-exp}}$ (mg/mL)	$q_{e\text{-cal}}$ (mg/mL)	k_1 (mg/(mL min))	R^2
10	0.4966	0.0441	0.0622	0.5076
25	1.2362	0.2367	0.0873	0.5750
50	2.4737	1.4322	0.1111	0.8906

Pseudo-second-order

c_0 (mg/L)	$q_{e\text{-exp}}$ (mg/mL)	$q_{e\text{-cal}}$ (mg/mL)	k_2 (mL/(mg min))	R^2
10	0.4966	0.4994	3.0861	0.9999
25	1.2362	1.2478	0.8743	0.9999
50	2.4737	2.5094	0.2779	1.0000

Elovich

c_0 (mg/L)	α (mg/(mL min))	β (mL/mg)	R^2
10	159.8091	24.1546	0.6045
25	179.0779	9.0827	0.7072
50	139.3733	4.1964	0.8431

$q_{e\text{-exp}}$ was calculated by the experiment data, and $q_{e\text{-cal}}$ was calculated by the adsorption kinetic models
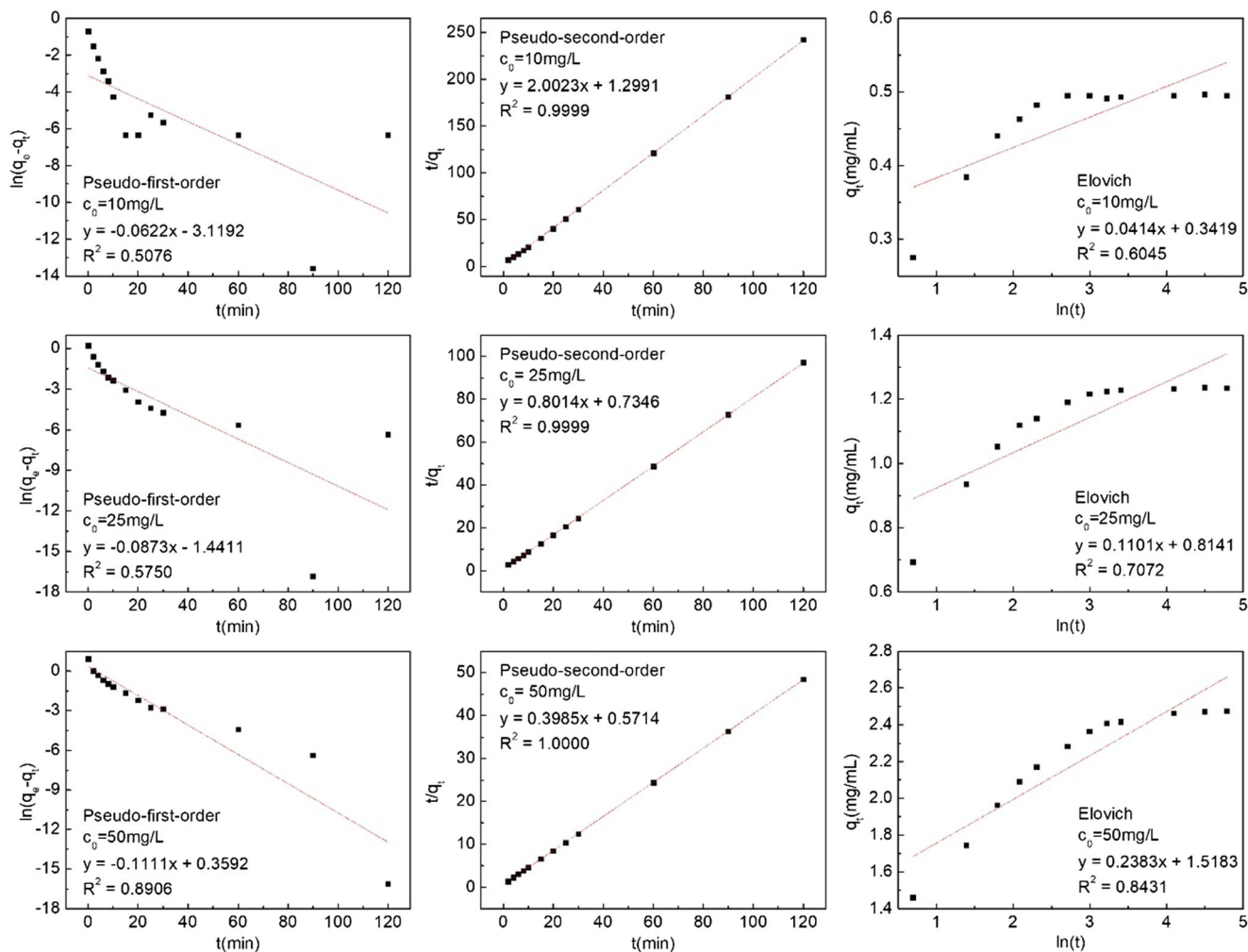

Fig. 4 The fitted curves of adsorption kinetics of P adsorption on MAEX resin. P concentrations were 10, 25, and 50 mg/L, resin dose was 20 mL/L, and volume of solution was 500 mL
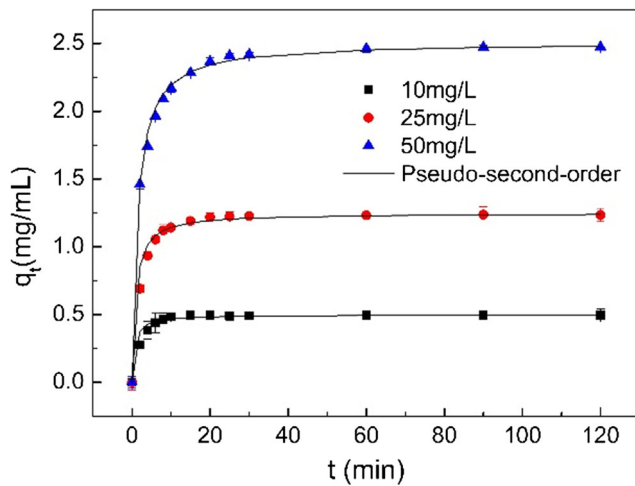
Fig. 5 Plots of pseudo-second-order model for P adsorption on MAEX resin. P concentrations were 10, 25, and 50 mg/L, resin dose was 20 mL/L, and volume of solution was 500 mL

reduction of P adsorption capacity on MAEX resin. As a result, the optimum pH for P adsorption by MAEX resin was 8.

From Fig. 3c, the increase of temperature was favorable to the P adsorption by MAEX resin, which indicated that the P adsorption process by MAEX resin might be an endothermic process. Besides, the P adsorption capacities of MAEX resin changed a little during the wide temperature range (283–323 K), which showed that the resin can deal well with the temperature change of the wastewater. In Fig. 3d, along with the concentration of sodium chloride increase from 0 to 1 mmol/L, the removal rate of P by MAEX resin decreased from 79.6 to 65%. It confirmed that the existence of Cl^- would reverse the original ion exchange equilibrium. As shown in Fig. 3e–g, the P adsorption capacities by MAEX resin were reduced in various degrees due to the interference of anions or organic compounds, which were mainly because of the competitive adsorption between anions or organic compounds and P. According to Table 4, we can conclude that pH was almost not changed after adding Cl^-, SO_4^{2-}, NO_3^-, and Br^-; however, pH was a little higher after adding CO_3^2 and HCO_3^-. The order of the inhibition of anion was as follows: $Br^- > SO_4^{2-} > Cl^- > NO_3^- > HCO_3^- >$

CO_3^{2-}. Compared Fig. 3 f and g, it was found that the inhibition of the humic acid was stronger than that of the bovine serum albumin. The reason may be that the humic acid has a smaller molecule than the bovine serum albumin (Liu et al. 2016), resulting in more easily adsorbed by MAEX resin.

Adsorption kinetics of P on MAEX resin

To investigate the mechanism and the dynamic of P adsorption process, several kinetic models (pseudo-first-order, pseudo-second-order, and Elovich equation) were tested to fit the experimental data obtained from the batch adsorption experiments (Hameed et al. 2007).

Adsorption kinetic models

Pseudo-first-order kinetic model has been widely used to describe the process of adsorption (Hameed et al. 2008). The equation is generally presented as follows:

$$\frac{dq_t}{dt} = k_1(q_e - q_t) \tag{5}$$

where k_1 stands for the rate constant of pseudo-first-order adsorption, q_e and q_t represent the adsorption capacity (mg/mL) at equilibrium and at any time, respectively. Integrating Eq. (5) with respect to boundary conditions $q = 0$ at $t = 0$ and $q = q_t$ at $t = t$, Eq. (5) becomes:

$$\ln(q_e - q_t) = \ln(q_e) - k_1 t \tag{6}$$

According to Eq. (6), the plot of ln $(q_e - q_t)$ versus t could fit a straight line. From the line, k_1 and q_e can be determined from the slope and intercept, respectively.

Pseudo-second order assumes that the rate-limiting step is chemisorption (Kan et al. 2017). The equation is generally presented as follows:

$$\frac{dq_t}{dt} = k_2(q_e - q_t)^2 \tag{7}$$

where k_2 stands for the rate constant of pseudo-second-order adsorption, q_e and q_t represent as same as above.

Table 6 Comparison of adsorption equilibrium time between some common adsorbents for P adsorption

Adsorbent	Initial P concentration (mg/L)	Adsorption kinetics	Adsorption equilibrium time	Reference
MAEX resin	25	Pseudo-second-order	30 min	This study
Ternary (Fe-Mg-Al)-layered hydroxides	20, 30	Pseudo-second-order	60 min	Liu et al. (2015)
Magnetic hydrotalcite-like compounds	50	Pseudo-second-order	24 h	Zhao (2007)
Biochars derived from dairy manure	20	Pseudo-second-order	4 h	Ma et al. (2015)
Lanthanum (III) loaded granular ceramic	10	Pseudo-second-order	30 h	Chen et al. (2012)
Modified rectorite	80–500	Pseudo-second-order	2 h	Xu et al. (2016)

Table 7 Constants and correlation coefficients of intraparticle diffusion model for P adsorption on MAEX

c_0 (mg/L)	k_{id1} (mg/(mL min$^{1/2}$))	C_1	R^2	k_{id2} (mg/(mL min$^{1/2}$))	C_2	R^2	k_{id3} (mg/(mL min$^{1/2}$))	C_3	R^2
10	0.1697	0.0178	0.9819	0.0047	0.4717	0.4077	0.0004	0.4914	0.4820
25	0.4407	0.0247	0.9908	0.0457	1.0047	0.9316	0.0014	1.2207	0.7802
50	0.7483	0.1510	0.9559	0.1323	1.7612	0.9850	0.0103	2.3690	0.8444

Integrating Eq. (7) and applying the initial conditions, Eq. (7) becomes:

$$\frac{t}{q_t} = \frac{1}{k_2 q_e^2} + \frac{1}{q_e} t \tag{8}$$

According to Eq. (8), the plot of t/q_t versus t could give a straight line. From the line, k_2 and q_e can be calculated from the slope and intercept, respectively.

Elovich equation, one of the most useful models, describes the kinetics of activated chemisorption process (Ali et al. 2016). The equation is generally presented as follows:

$$q_t = \frac{1}{\beta} \ln(\alpha\beta) - \frac{1}{\beta} \ln(t) \tag{9}$$

From Eq. (9), α and β are the constants obtained from the slope and intercept of the linear plot of q_t versus ln (t).

Analysis of the experimental data

The adsorption kinetic parameters on MAEX resin at different initial P concentrations were given in Table 5, and the fitted curves for different systems were shown in Fig. 4. According to Table 5, the adsorption process most closely followed pseudo-second-order kinetics, by which the highest correlation coefficient ($R^2 > 0.99$) was obtained as well as the very accurate estimation of q_e. From Fig. 4, we also could find that pseudo-second-order kinetic curves appeared to fit well with the experimental data. This suggested that the adsorption of P on MAEX resin may be controlled by the chemical sorption, which involved covalent forces through exchanging or sharing the electrons between adsorbate and adsorbent (Wang et al. 2018). According to Fig. 5, the main process of adsorption was completed in 30 min and the P adsorption capacity at 30 min could reach 97.7–99.3% of q_e. Table 6 showed us the comparison of adsorption equilibrium time between some common adsorbents for P adsorption. We could deduce that the P adsorption by MAEX resin reached to equilibrium within a very short time, resulting in shortening treatment time and improving efficiency of wastewater treatment.

Intraparticle diffusion model and analysis

The adsorption process is controlled by several steps including (i) diffusion of the solute from solution to the film on particle surfaces, (ii) diffusion from the film to the particle surface after overcoming liquid film resistance (external diffusion), (iii) diffusion from the surface to the active adsorption sites on the inner surface of particles (surface diffusion or pore diffusion), and (iv) uptake which can involve several mechanisms such as ion exchange, physicochemical sorption, complexation, or precipitation (Wu et al. 2001; Gercel et al. 2007).

Adsorption kinetics is usually controlled by different mechanisms, of which the most limiting ones are the diffusion mechanisms (Toor and Jin 2012). As the diffusion mechanism cannot be identified by the above kinetic models, the intraparticle diffusion model based on the theory proposed by Weber and Morris was widely studied (Weber and Morris 1963). This model assumes that diffusion controls the sorption process if the whole reaction rate is dependent upon the diffuse rate between adsorbate and adsorbent. The model was characterized by Eq. (10):

$$q_t = k_{id} t^{1/2} + C \tag{10}$$

where k_{id} is the intraparticle rate constant (mg/(g·s t$^{1/2}$)) and C is the intercept. According to Eq. (10), the plot of q_t versus $t^{1/2}$ should be linear. If this line passed through the origin, the intraparticle diffusion is the rate-limiting step to the adsorption process. If not, there are other factors controlling the process, such as liquid film (Bhattacharyya and Gupta 2006).
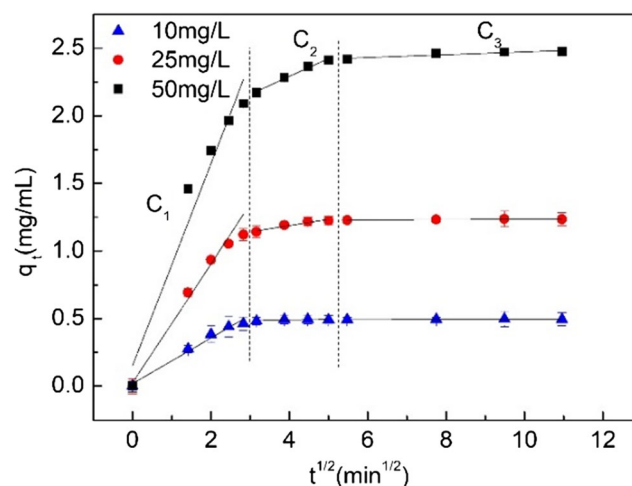

Fig. 6 Plots of intraparticle diffusion model for P adsorption on MAEX resin. P concentrations were 10, 25, and 50 mg/L, resin dose was 20 mL/L, and volume of solution was 500 mL

Table 8 Constants and correlation coefficients of Langmuir and Freundlich models

T(K)	Isotherm model					
	Langmuir			Freundlich		
	q_m (mg/mL)	K_L (L/mg)	R^2	K_F (mg/mL)	n	R^2
293	2.3153	2.8546	0.9741	21.0334	0.1106	0.6103
303	2.3408	4.1516	0.9886	28.7237	0.1107	0.6457
313	2.4038	11.5236	0.9982	78.2220	0.1068	0.6956

Table 7 presented the constants and the correlation coefficients of intraparticle diffusion model for P adsorption on MAEX resin, while Fig. 6 showed the adsorption profiles by plotting q_t versus $t^{1/2}$ for three initial P concentrations.

As illustrated in Fig. 6, during the whole reaction time, the adsorption process was divided into three different stages:

(i) The first stage was surface adsorption stage at the initial adsorption, by which the linear slope was the largest and the adsorption rate was the fastest. During this stage, the process of P transferring from the solution to the adsorbent surface was the mainly material transfer process which had a small resistance.

(ii) The next stage was the internal diffusion process. At this time, the adsorption on the adsorbent surface was basically completed with gradually smaller adsorption rate, and the adsorption process started to transfer into the holes of adsorbent.

(iii) The final stage was the adsorption saturation process, where the adsorption capacity of adsorbent was no longer changed with time, indicating that the adsorption process had reached saturation.

Although there was a high correlation coefficient between q_t and $t^{1/2}$ as shown in Table 7, the fitting curves were not through the coordinate origin at different stages of the adsorption process. It indicated that the adsorption reaction was mainly not only controlled by intraparticle diffusion, while the adsorption rate was also affected by particle diffusion, such as surface adsorption or liquid film diffusion. These three diffusion stages have also been observed form another P-adsorption process in which the soils from diverse ecological zones were used as the adsorbent (Zhang et al. 2015).

Adsorption thermodynamic characteristics of P on MAEX resin

Adsorption isotherm models and analysis

Adsorption isotherm is the equilibrium curve describing the relationship between the adsorbate in solution and adsorbate adsorbed on the surface of adsorbent at a given temperature (Treybal 1981). Establishing the most appropriate correlation for the equilibrium curves is important to optimize the design of an adsorption system (Hameed et al. 2008).

In this study, two adsorption isotherms, namely, Langmuir and Freundlich isotherms, were applied to the equilibrium data of P adsorption on MAEX resin.

The widely used Langmuir isotherm has found successful application in many real sorption processes (Agyei et al. 2000; Bajpai et al. 2000). Langmuir isotherm model is valid for mono-layer sorption on a surface with a finite number of identical sites and is generally expressed as follow (Sheshdeh et al. 2014):

$$q_e = \frac{q_m K_L c_e}{1 + K_L c_e} \qquad (11)$$

$$\frac{1}{q_e} = \frac{1}{q_m} + \frac{1}{q_m K_L} \times \frac{1}{c_e} \qquad (12)$$

In the above equations, c_e and q_e are respectively the concentration of adsorbate (mg/L) and the adsorption capacity of adsorbent (mg/mL) at equilibrium, q_m stands for Langmuir sorption capacity (mg/mL), and K_L is the parameter of
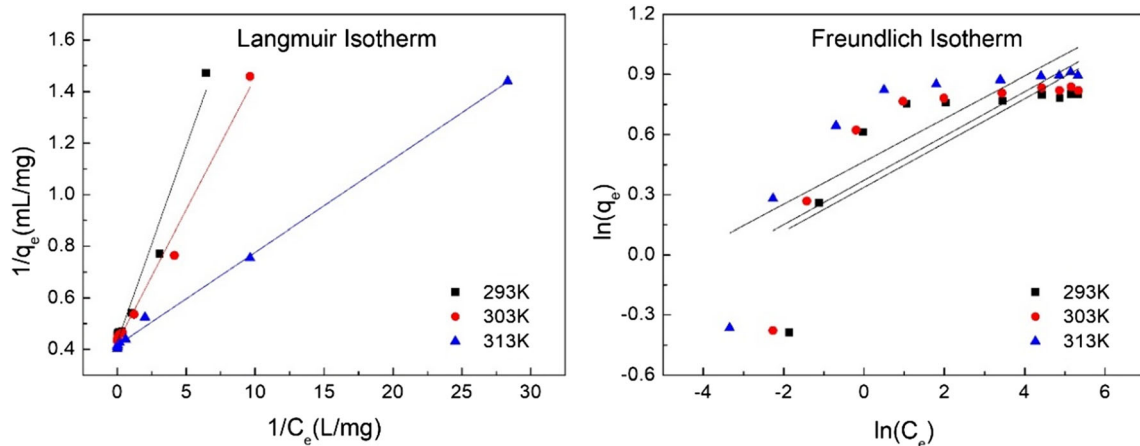

Fig. 7 The fitting of adsorption data on the Langmuir and Freundlich models. Temperatures were 293 K, 303 K, and 313 K, resin dose was 8 mL/L, and initial pH was 8
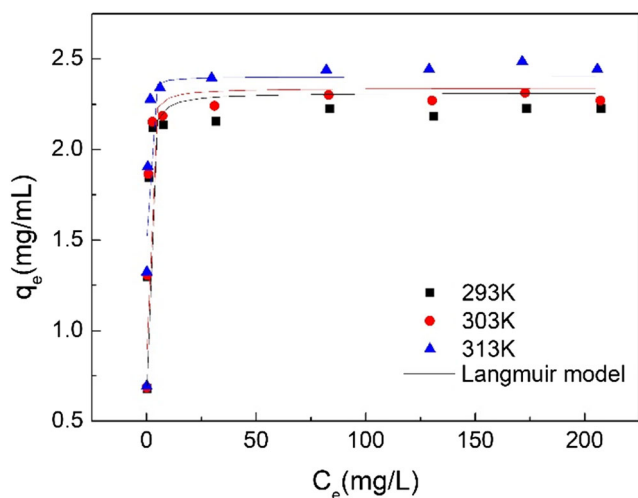
Fig. 8 Plots of Langmuir model for P adsorption on MAEX resin. Temperatures were 293 K, 303 K, and 313 K, resin dose was 8 mL/L, and initial pH was 8

Langmuir isotherm equation which can reflect adsorption capacity of adsorbent.

Freundlich isotherm is often used for heterogeneous surface energy systems (Agyei et al. 2000; Baup et al. 2000). The equation is expressed as follow:

$$q_e = K_F c_e^{1/n} \tag{13}$$

where K_F is the parameter of Freundlich isotherm equation which is related to binding energy and adsorption capacity. The shape of the isotherm depends on the value of $1/n$ as follows (Toor and Jin, 2012): the isotherm is unfavorable ($1/n > 1$), ineffective ($1/n = 1$), favorable ($0 < 1/n < 1$), or reversible ($1/n = 0$).

The parameters of Langmuir and Freundlich isotherm models at three temperatures were listed in Table 8, while
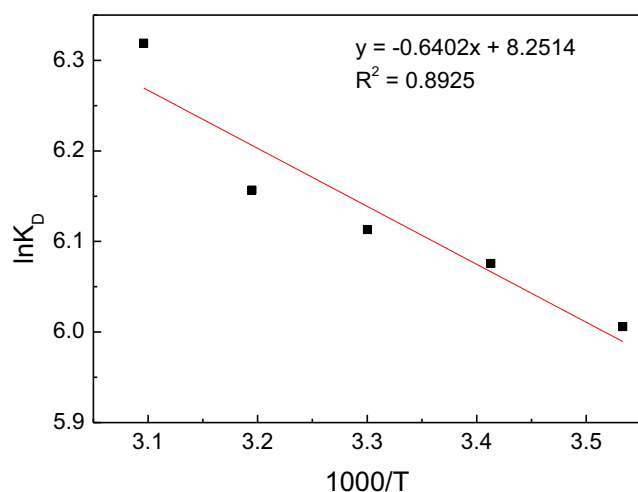
Table 9 Thermodynamics parameters of P adsorption on MAEX resin

T(K)	ΔG (kJ/mol)	ΔH (kJ/mol)	ΔS (J/(mol·K))
283	− 14.1309	5.3226	68.6021
293	− 14.8004		
303	− 15.3995		
313	− 16.0213		
323	− 16.9689		

Figs. 7 and 8 described the fitting curves of two isotherm models. As shown in Table 8 and Fig. 7, Langmuir model with the higher regression coefficients than those of Freundlich model was more suitable for the adsorption behaviors of P on MAEX resin. This indicated that adsorption of P is a monolayer adsorption on the surface of MAEX resin. Furthermore, as presented in Fig. 8, there were no significant increases in the equilibrium adsorption capacity of P when the initial P concentration reached to 50 mg/L, further proving the formation of monolayer coverage of P at the surface of MAEX resin. Similar phenomenon was observed in the adsorption of P on Fe_3O_4 magnetic nanoparticles (Li et al., 2013), ternary (Fe-Mg-Al)-layered hydroxides (Liu et al. 2015), and modified rectorite (Xu et al. 2016). However, some studies found that the Freundlich model gave a better fit on the adsorption of P using different adsorbents (Shen and Huang 2011; Kuwahara et al. 2016). This might be affected by the characteristics of the adsorbents chosen.

Adsorption thermodynamic parameters

The thermodynamic parameters, such as standard free energy (ΔG), enthalpy (ΔH), and entropy (ΔS), could be helpful to further explain the mechanism of adsorption process (Sarkar et al. 2017). These parameters can be determined from the

Fig. 9 Plots of ln (K_D) versus $1/T$ for P adsorption on MAEX resin. P concentrations was 25 mg/L; resin dose was 8 mL/L; initial pH was 8; and temperatures were 283 K, 293 K, 303 K, 313 K, and 323 K
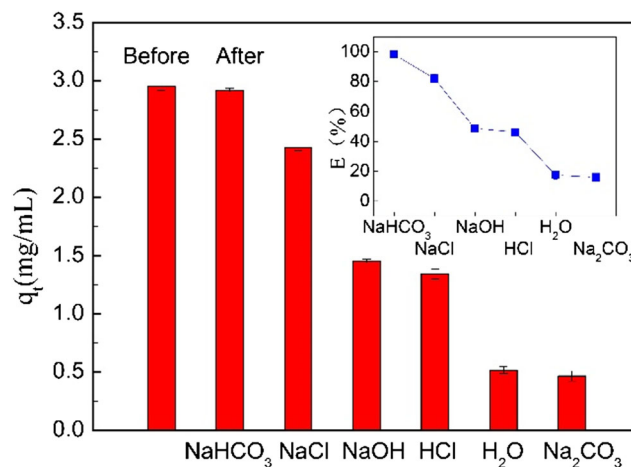

Fig. 10 The adsorption capacities of MAEX before and after different regenerations. P concentration was 25 mg/L, resin dose was 8 mL/L, and regeneration concentration was 1.0 mol/L
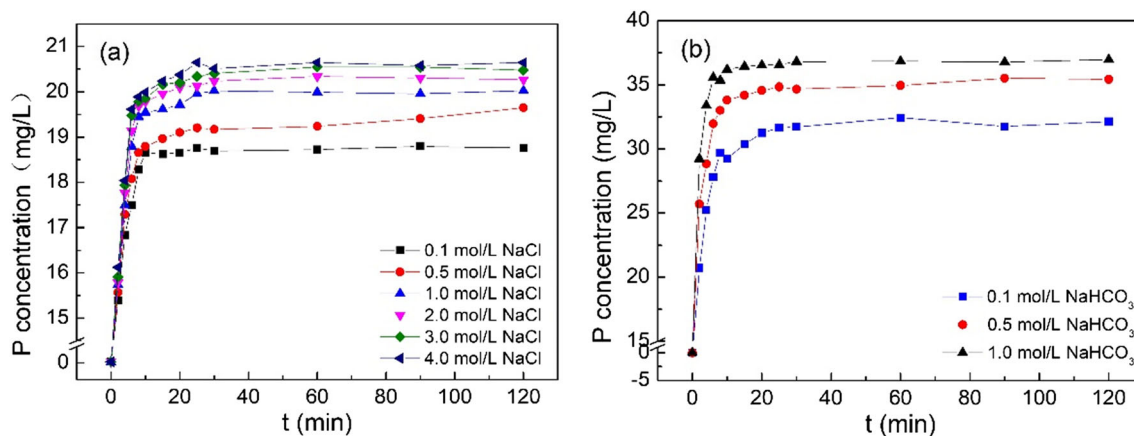
Fig. 11 Comparison of regeneration kinetics of MAEX resin by NaCl and NaHCO$_3$ with different concentrations

following equations:

$$\Delta G = -RT \ln K_D \tag{14}$$

$$\ln K_D = \Delta S / R - \Delta H / RT \tag{15}$$

In Eqs. (14) and (15), R is the gas constant (8.314 J/mol K), T is the temperature (K), and K_D is the standard thermodynamic equilibrium constant (L/mol) which is calculated by Eq. (16):

$$K_D = \frac{C_0 - C_t}{C_t} \times \frac{V}{W} \tag{16}$$

In Eq. (16), C_0 is the initial P concentration (mg/L), C_t is the P concentration (mg/L) in the solution at equilibrium, V is volume of the solution (mL), and W is dosage of MAEX resin (mL). The detailed computation processes of thermodynamic parameters are as follows: (i) calculating the values of K_D at different temperatures, (ii) linear fitting of $\ln K_D$ versus $1/T$ (Fig. 9), (iii) calculating ΔS and ΔH from the slope and the

intercept, respectively, and (iv) determining ΔG at different temperatures.

From Table 9, the positive value of ΔH (5.3226 KJ/mol) denoted that the adsorption reaction was endothermic, which was also proved by Fig. 3c. The positive value of ΔS (68.6021 J/(mol·K)) suggested that the degree of confusion on the solid-liquid interface was increased and the adsorption reaction can be carried out spontaneously. The value of ΔS was positive, which indicates that the dissociative mechanism was involved in the sorption process. (Abbasizadeh et al., 2014; Talebi et al., 2017). The values of ΔG at different temperatures were all negative (range from − 14.1309 to − 16.9689 KJ/mol), further indicating that the adsorption process of P on MAEX resin was spontaneous thermodynamically. Moreover, as the increase of temperature, the value of ΔG decreases gradually, which showed that increasing of temperature is beneficial to the adsorption process of P on MAEX resin. Besides, according to the absolute value of ΔG at five temperatures ranged from 14 to 17 KJ/mol, we could infer that the adsorption is not only chemical adsorption, but also physical adsorption.
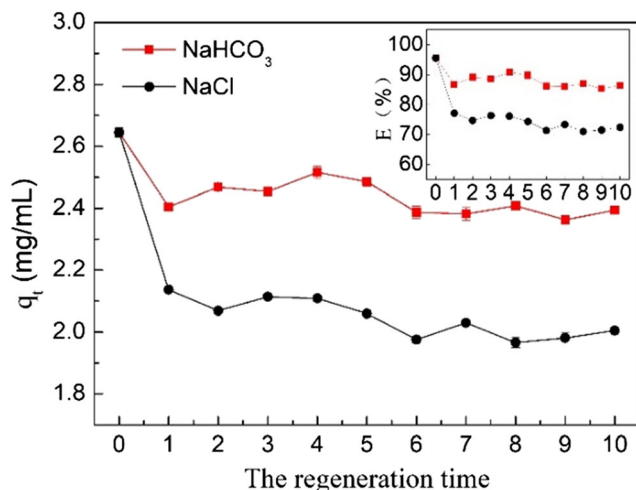
Regeneration and reuse of MAEX resin

Figure 10 showed the regeneration effects of MAEX by different reagents. As seen, the order of the regenerative ability was as follows: NaHCO$_3$>NaCl>NaOH>HCl>H$_2$O>Na$_2$CO$_3$, while the adsorption capacities of MAEX resin after regeneration were respectively 98.12%, 82.04%, 48.74%, 46.34%, 17.43%, and 15.97% of the original capacities. The result showed that NaHCO$_3$ and NaCl have good performance on MAEX resin regeneration, indicating that chloride (Cl$^-$) and bicarbonate (HCO$_3$$^-$) could exchange phosphate at the surface reaction sites of resin more effectively. Cl$^-$ at the surface of the resin is the functional point which can exchange the contaminant ions from solution. In addition, OH$^-$ hydrolyzed by HCO$_3$$^-$ might be reacted with H$_2$PO$_4$$^-$ or HPO$_4$$^{2-}$ and formed

Fig. 12 Effect of regeneration times on the removal of phosphorus. Initial P concentration was 25 mg/L, and MAEX resin dose was 20 mL/L

Table 10 Comparison of P adsorption by different adsorbents after multiple regeneration

Adsorbent	Reagent	Times of adsorption-desorption cycles	q_R/q_0*	Reference
MAEX resin	NaHCO$_3$	10	90.51%	This study
BA-Fe-Al magnetic zeolite	NaOH	6	64.8%	Jiang (2016)
TMA-Fe-Al magnetic zeolite	NaOH	6	75.1%	Jiang (2016)
PMA-Fe-Al magnetic zeolite	NaOH	6	77.4%	Jiang (2016)
Mn-Fe magnetic zeolite	NaOH	6	66.7%	Jiang (2016)
Zr-Fe magnetic zeolite	NaOH	6	64.2%	Jiang (2016)
Mn-Zr-Fe magnetic zeolite	NaOH	6	76.8%	Jiang (2016)
CMC-CoFe$_2$O$_4$	NaCl	1	88.92%	Xu (2013)
Ferric salt modified oyster shell	HCl	8	88%	Wang (2012)

*q_R was the adsorption capacity of adsorbent after the last regeneration in this table

to PO$_4^{3-}$, leading to the charge increasing of phosphate ions, which promoted P adsorption on MAEX resin.

Figure 11 depicted the regeneration process of MAEX resin by NaCl and NaHCO$_3$ with different concentrations. From Fig. 11a, P desorbed from MAEX resin was basically stable after 30 min of reacting and increased as the increasing of NaCl concentration. When the concentration of NaCl increased from 0.1 to 1.0 mol/L, the concentration of P in the solution increased from 18.76 to 20.03 mg/L. However, when the concentration of NaCl continued increasing until 4.0 mol/L, the concentration of P just increased to 20.64 mg/L, with no visible difference. Therefore, 1.0 mol/L of NaCl was suitable for the regeneration process of resin. As for Fig. 11b, when the concentration of NaHCO$_3$ increased from 0.1 to 1.0 mol/L, the concentration of P in the solution desorbed from the resin increased from 32.13 to 36.97 mg/L. Since 1.0 mol/L is close to the solubility of NaHCO$_3$ at the room temperature, 1.0 mol/L of NaHCO$_3$ was chased for the subsequent adsorption-desorption cycle experiments.

Figure 12 showed us the adsorption capacities of MAEX resin during ten times of adsorption-desorption cycle experiments by NaHCO$_3$ and NaCl. After ten times of regeneration by 1.0 mol/L NaHCO$_3$ and NaCl, the adsorption capacities of MAEX resin reduced by 9.48% and 24.2%, respectively. The removal rates of P after ten times of regeneration by NaHCO$_3$ and NaCl were 90.51% and 75.8% of the original rate, respectively. The result showed that the regenerating performance of NaHCO$_3$ was better than that of NaCl. Furthermore, no significant loss of adsorption capacity of MAEX resin was observed after 10 cycles of adsorption-desorption, indicating that MAEX resin could be reused for many times and MAEX resin has good physical stability. Table 10 was the comparison of P adsorption by the MAEX resin and with other adsorbents after multiple regeneration. According to Table 10, we could conclude that MAEX resin had little adsorption capacity loss after 10 cycles of adsorption-desorption and had a high

regeneration efficiency, which can save the cost of P removal from wastewater.

Characterization of MAEX resin before and after adsorption

FTIR could provide detailed information about the change of ions and functional groups in resin. As shown in Fig. 13, there were obvious absorption bands appeared at 1074 cm^{-1}, 968 cm^{-1}, and 634 cm^{-1}, while the absorption bands around 1070 cm^{-1}, 970 cm^{-1}, and 630 cm^{-1} were respectively attributed to PO$_4^{3-}$ and HPO$_4^{2-}$ (Weng 2010), indicating that MAEX resin had an effective adsorption of P in the solution. The absorption band around 463 cm^{-1} (the symmetrical telescopic vibration band of C–Cl) (Weng 2010) decreased significantly after adsorption, which represented that the content of chloride in MAEX resin decreased, presumably since the chloride was exchanged by P and transferred into solution. In addition, the absorption bands around 3400 cm^{-1} to 3230 cm^{-1} and 3075 cm^{-1} to 3030 cm^{-1}, attributed to the
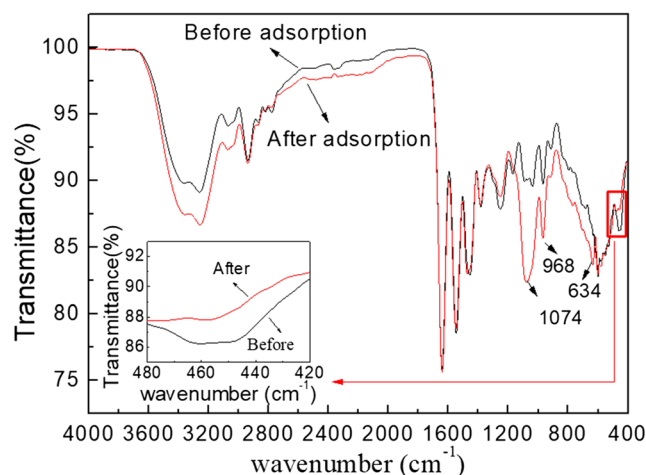

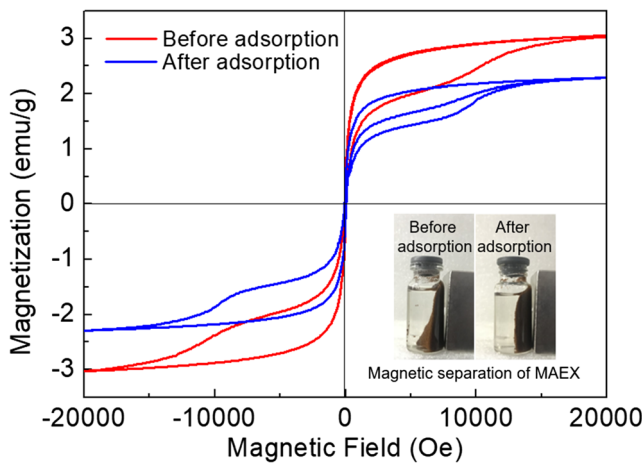**Fig. 13** The FTIR spectra of MAEX resin before and after adsorption

Fig. 14 The VSM curves of MAEX resins before and after adsorption

stretching vibration of alcoholic hydroxyl (Liu et al. 2018) and symmetric stretching vibration of ammonia (Ma et al. 2005), respectively, shifted or changed the intensity after adsorption, which implied that, besides ion exchange, there are other adsorptions (e.g., charge attraction and hydrogen bonding) which affected the removal of P by MAEX resin.

The magnetic hysteresis loop describing the magnetization versus magnetic field was presented in Fig. 14. The coercive force (Hc) value of original MAEX resin was 58.22 Oe (0.73 A/m). According to the value of coercive force, the ferromagnetic materials are divided into soft magnetic materials with low coercive force ($Hc < 102$ A/m) and hard magnetic materials with high coercive force ($Hc > 102$ A/m) (Li 2014), explaining that MAEX resin is a kind of soft magnetic materials. Moreover, the saturation magnetization (Ms) values of MAEX resins before and after adsorption were 3.05 emu/g and 2.62 emu/g, respectively. Although the value of Ms

decreased slightly after adsorption, the resin still had good magnetic properties and did not affect the application of MAEX resin.

Adsorption mechanism

Based on the results of kinetics, thermodynamics, and infrared analysis, it could be speculated that during the initial stage of adsorption, ion exchange had acted a leading role since there were enough active ion-exchange sites on the surface of the resin to exchange P from the solution. However, along with reacting, the limited active ion-exchange sites could not meet the need for adsorption of P. Once the adsorption reach to the saturation state of monomolecular adsorption, MAEX resin adsorbed P mainly through Van der Waals force and hydrogen bond. Nevertheless, compared with ion exchange, the reaction rate of physical adsorption was slower. The adsorption reaction would proceed slowly until reaching the saturation adsorption (shown in Fig. 15).

Conclusions

This work demonstrated that MAEX resin has a high phosphorus removal and recovery potential. Compared with traditional anion exchange resins, the MAEX resin had a stable magnetic property, which made it easy to aggregate and settle from water after adsorption. An important finding was that temperature had little effect on the adsorption capacity of P on MAEX resin, which illustrated this resin had a good P removal efficient in a wide range of temperature and could be used against the temperature fluctuation of wastewater in
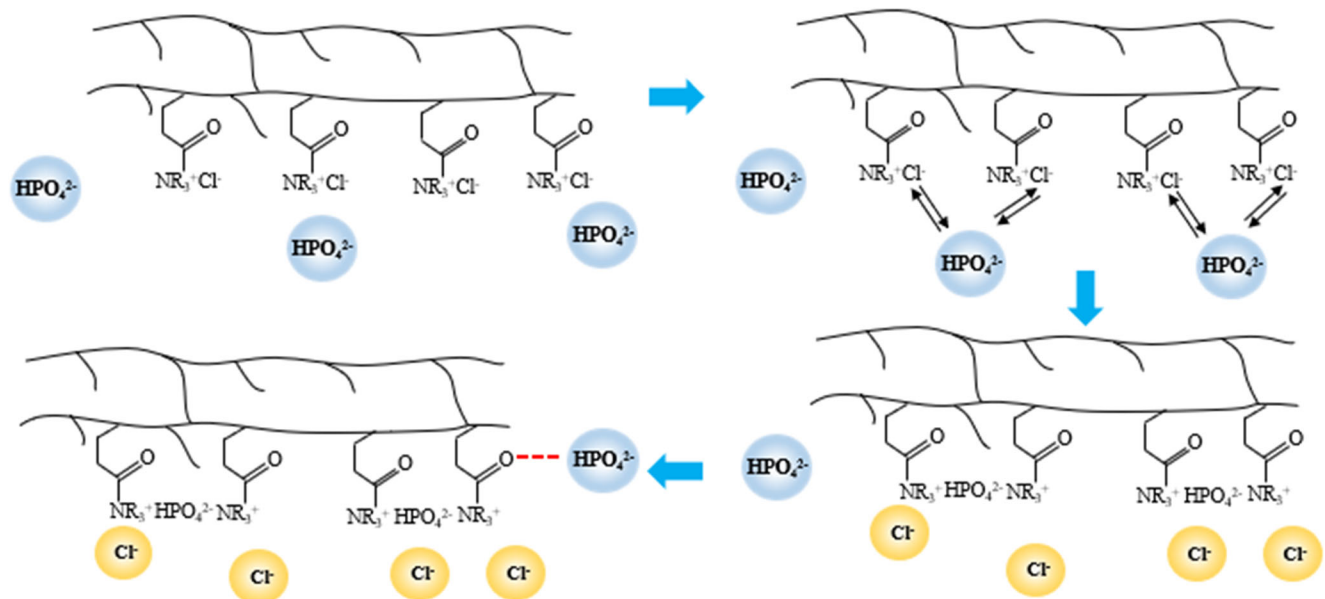

Fig. 15 The sketch map of the P adsorption process by MAEX resin

some circumstance. The MAEX resin had a rapid adsorption rate of P comparing with the other adsorbents. In addition, this resin could be successfully regenerated and had little adsorption capacity loss after 10 cycles of adsorption-desorption, which could reduce the overall cost of P removal.

All these results revealed that MAEX resin was a promising adsorbent in removing P from wastewater. Further work aiming at the evaluation of P removal effect in actual sludge dewatering filtrate and deep exploring of P adsorption mechanism by MAEX resin is currently in progress.

Publisher's Note Springer Nature remains neutral with regard to jurisdictional claims in published maps and institutional affiliations.

References

Abbasizadeh S, Keshtkar AR, Mousavian MA (2014) Sorption of heavy metal ions from aqueous solution by a novel cast PVA/TiO$_2$ nanohybrid adsorbent functionalized with amine groups. J Ind Eng Chem 20:1656–1664

Agyei NM, Strydom CA, Potgieter JH (2000) An investigation of phosphate ion adsorption from aqueous solution by fly ash and slag. Cem Concr Res 30(5):823–826

Ali RM, Hamad HA, Hussein MM, Malash GF (2016) Potential of using green adsorbent of heavy metal removal from aqueous solutions: adsorption kinetics, isotherm, thermodynamic, mechanism and economic analysis. Ecol Eng 91:317–332

Bajpai AK, Rajpoot M, Mishra DD (2000) Static and kinetic studies on the adsorption behavior of sulfadiazene. Adsorption 6(4):349–357

Baup S, Jaffre C, Wolbert D, Laplanche A (2000) Adsorption of pesticides onto granular activated carbon: determination of surface diffusivities using simple batch experiments. Adsorption 6(3):219–228

Bhatnagar A, Sillanpää M (2011) A review of emerging adsorbents for nitrate removal from water. Chem Eng J 168(2):493–504

Bhattacharyya KG, Gupta SS (2006) Adsorption of Fe (III) from water by natural and acid activated clays: studies on equilibrium isotherm, kinetics and thermodynamics of interactions. Adsorption 12(3):185–204

Boyer TH, Singer PC (2005) Bench-scale testing of a magnetic ion exchange resin for removal of disinfection by-product precursors. Water Res 39(7):1265–1276

Chen N, Feng CP, Zhang ZY, Liu RP, Gao Y, Li M, Sugiura N (2012) Preparation and characterization of lanthanum (III) loaded granular ceramic for phosphorus adsorption from aqueous solution. J Taiwan Inst Chem E 43(5):783–789

Chitrakar R, Tezuka S, Sonoda A, Sakane K, Ooi K, Hirotsu T (2005) Adsorption of phosphate from seawater on calcined MgMn-layered double hydroxides. J Colloid Interface Sci 290(1):45–51

Chitrakar R, Tezuka S, Sonoda A, Sakane K, Ooi K, Hirotsu T (2006) Selective adsorption of phosphate from seawater and wastewater by amorphous zirconium hydroxide. J Colloid Interface Sci 297(2):426–433

Chouyyok W, Wiacek RJ, Pattamakomsan K, Sangvanich T, Grudzien RM, Fryxell GE, Yantasee W (2010) Phosphate removal by anion binding on functionalized nanoporous sorbents. Environ Sci Technol 44(8):3073–3078

Sartorius C, Von HJ, Tettenborn F (2012) Phosphorus recovery from wastewater—expert survey on present use and future potential. Water Environ Res 84(4):313–322

Dai J, Yang H, Yan H, Shangguan Y, Zheng Q, Cheng R (2011) Chem Eng JPhosphate adsorption from aqueous solutions by disused adsorbents: chitosan hydrogel beads after the removal of copper (II). Chem Eng J 166(3):970–977

Ding L, Wu C, Deng H, Zhang XX (2012) Adsorptive characteristics of phosphate from aqueous solutions by MIEX resin. J Colloid Interface Sci 376(1):224–232

Roy ED (2017) Phosphorus recovery and recycling with Ecol Eng: A review. Ecol Eng 98:213–227

Gan F, Zhou J, Wang H, Du C, Chen X (2009) Removal of phosphate from aqueous solution by thermally treated natural palygorskite. Water Res 43(11):2907–2915

Gercel O, Ozcan A, Ozcan AS, Gercel HF (2007) Preparation of activated carbon from a renewable bio-plant of *Euphorbia rigida* by H$_2$SO$_4$ activation and its adsorption behavior in aqueous solutions. Appl Surf Sci 253(11):4843–4852

Hameed BH, Ahmad AA, Aziz N (2007) Isotherms, kinetics and thermodynamics of acid dye adsorption on activated palm ash. Chem Eng J 133(1):195–203

Hameed BH, Tan IAW, Ahmad AL (2008) Adsorption isotherm, kinetic modeling and mechanism of 2,4,6-trichlorophenol on coconut husk-based activated carbon. Chem Eng J 144(2):235–244

Hao XD, Yi LK, Wang CC, Qiu FG (2010) Situation and prospects pf phosphorus recovery techniques. J Environ Sci-China 30(5):897–907

Huang W, Wang S, Zhu Z, Li L, Yao X, Rudolph V, Haghseresht F (2008) Phosphate removal from wastewater using red mud. J Hazard Mater 158(1):35–42

Jiang L (2016) Performance and mechanism of aqueous phosphorus removal by magnetic zeolite. Dissertation, Anhui University of Technology

Kan CC, Ibe AH, Rivera KKP, Arazo RO, Luna MDGD (2017) Hexavalent chromium removal from aqueous solution by adsorbents synthesized from groundwater treatment residuals. Sus Env Res 27(4):163–171

Kitis M, Harman BI, Yigit NO, Beyhan M, Nguyen H, Adams B (2007) The removal of natural organic matter from selected Turkish source waters using magnetic ion exchange resin (MIEX®). React Funct Polym 67(12):1495–1504

Kuwahara Y, Tamagawa S, Fujitani T, Yamashita H (2016) Removal of phosphate from aqueous solution using layered double hydroxide prepared from waste iron-making slag. Bull Chem Soc Jpn 89(4):472–480

Li JM (2014) The investigations on the electrochemical fabrication and related properties of nanocrystalline magnetic thin films. Dissertation, Shanghai Jiao Tong University

Li Y, Zhao XL, Huang YM (2013) The adsorptive removal of phosphorus by Fe$_3$O$_4$ magnetic nanoparticles as an adsorbent. J Southwest Univ N 35(5):127–130

Liu G, Li J, Yang X, Han GR (2015) Study on the adsorption capacity of ternary (Fe-Mg-Al) layered hydroxides for phosphorus. Ind Water Treat 35(1):62–64

Liu W, Yan XD, Wu M, Sun MX, Liu HY, Dai J (2016) Fluorescence spectroscopy analysis of domestic wastewater based on molecular weight distribution. Hubei Agric Sci 55(4):872–877

Liu X, Chen ZQ, Han B, Su CL, Han Q, Chen WZ (2018) Biosorption of copper ions from aqueous solution using rape straw powders: optimization, equilibrium and kinetic studies. Ecotoxicol Environ Saf 150:251–259

Liu ZQ, Yan XM, Drikas M, Zhou DN, Wang DS, Yang M, Qu JH (2011) Removal of bentazone from micro-polluted water using MIEX resin: kinetics, equilibrium, and mechanism. J Environ Sci 23(3):381–387

Loganathan P, Vigneswaran S, Kandasamy J, Bolan NS (2014) Removal and recovery of phosphate from water using sorption. Crit Rev Environ Sci Technol 44(8):847–907

Lwin CM, Murakami M, Hashimoto S (2017) The implications of allocation scenarios for global phosphorus flow from agriculture and wastewater. Resour Cnsv Recycl 122:94–105

Ma FF, Zhao BW, Zhong JK, Diao JR, Zhang Y (2015) Characteristics phosphate adsorption onto biochars derived from dairy manure and its influencing factors. China Environ Sci 35(4):1156–1163

Ma ZY, Guan YP, Liu HZ (2005) Synthesis and characterization of micron-sized monodisperse superparamagnetic polymer particles with amino groups. J Polym Sci A Polym Chem 43(15):3433–3439

Mergen MR, Jefferson B, Parsons SA, Jarvis P (2008) Magnetic ion-exchange resin treatment: impact of water type and resin use. Water Res 42(8–9):1977–1988

Morse GK, Brett SW, Guy JA, Lester JN (1998) Review: phosphorus removal and recovery technologies. Sci Total Environ 212(1):69–81

Ozacar M (2003) Adsorption of phosphate from aqueous solution onto alunite. Chemosphere 51(4):321–327

Ozmen F, Kavakli PA, Guven O (2011) Removal of phosphate by using copper-loaded poly (N-vinylimidazole) hydrogels as polymeric ligand exchanger. J Appl Polym Sci 119(1):613–619

Sarkar K, Sen K, Lahiri S (2017) Radiometric analysis of isotherms and thermodynamic parameters for cadmium (II) adsorption from aqueous medium by calcium alginate beads. J Radioanal Nucl Chem 312(4):1–12

Schütte T, Niewersch C, Wintgens T, Yüce S (2015) Phosphorus recovery from sewage sludge by nanofiltration in diafiltration mode. J Membr Sci 480:74–82

Shen W, Huang H (2011) Study on phosphorus in municipal wastewater adsorbed by sulfuric acid-activated coal-measures kaoline. Coal Convers 34(1):78–61

Sheshdeh RK, Abbasizadeh S, Nikou MRK, Badii K, Sharafi MS (2014) Liquid phase adsorption kinetics and equilibrium of toluene by novel modified-diatomite. J Environ Health Sci Eng 12:148

Shih YJ, Abarca RRM, MDG d L, Huang YH, Lu MC (2017) Recovery of phosphorus from synthetic wastewaters by struvite crystallization in a fluidized-bed reactor: effects of pH, phosphate concentration and coexisting ions. Chemosphere 173:466–473

Song MY, Li M, Liu JJ (2017) Uptake characteristics and kinetics of inorganic and organic phosphorus by *Ceratophyllum demersum*. Water Air Soil Pollut 228(11):407

Talebi M, Abbasizadeh S, Keshtkar AR (2017) Evaluation of single and simultaneous thorium and uranium sorption from water systems by an electrospun PVA/SA/PEO/HZSM5 nanofiber. Process Saf Environ Prot 109:340–356

Toor M, Jin B (2012) Adsorption characteristics, isotherm, kinetics, and diffusion of modified natural bentonite for removing diazo dye. Chem Eng J 187(2):79–88

Treybal ER (1981) Mass transfer operations. McGraw-Hill International editions, Singapore

Ugurlu A, Salman B (1998) Phosphorus removal by fly ash. Environ Int J Environ Sci Risk Health 24(8):911–918

Wang SD, Kong LJ, Long JY, Su MH, Diao ZH, Chang XY, Chen DY, Song G, Shih K (2018) Adsorption of phosphorus by calcium-flour biochar: Isotherm, kinetic and transformation studies. Chemosphere 195:666–672

Wang YX (2012) Study on phosphorus recovery from excess sludge by ferric salt modified oyster shell. Dissertation, Dalian University of Technology

Weber WJ, Morris JC (1963) Kinetics of adsorption on carbon from solution. Asce Sanit Eng Div J 1(2):1–2

Weng SP (2010) Fourier transform infrared spectrometric analysis. Chemical Industry Press, Beijing

Wu FC, Tseng RI, Jung RS (2001) Kinetic modeling of liquid-phase adsorption of reactive dyes and metal ions on chitosan. Water Res 35(3):613–618

Xu GY, Yin HQ, Hu JL, Sun QW (2016) Studies on the preparation of modified rectorite and its adsorbing performance for phosphorus in water. Chem Res Appl 28(07):1025–1029

Xu XM (2013) Synthesis of magnetic CMC-CoFe$_2$O$_4$ compounds and research on the phosphate removal and recovery from wastewater. Dissertation, Harbin Engineering University

Xu Y, Peng H, Yang Y, Zhang Y, Wang S (2014) A cumulative eutrophication risk evaluation method based on a bioaccumulation model. Ecol Model 289(289):77–85

Yuan ZG, Pratt S, Batstone DJ (2012) Phosphorus recovery from wastewater through microbial processes. Curr Opin Biotechnol 23(6):878–883

Zhang L, Loáiciga HA, Xu M, Du C, Du Y (2015) Kinetics and mechanisms of phosphorus adsorption in soils from diverse ecological zones in the source area of a drinking-water reservoir. Int J Environ Res Public Health 12(11):14312–14326

Zhao BQ (2007) Study on adsorption and recovery of phosphate by magnetic hydrotalcite-like compounds in aqueous solution. Dissertation, Harbin Institute of Technology